Mem. Fac. Eng., Kyoto Univ., Vol. 56, No. 3 (1994)

Silicon-based 2 Terminal Tandem Solar Cells with Lattice-Matched Buffer Layers

By

Yuji KOMATSU, Takashi FUYUKI, Hiroyuki MATSUNAMI

(Received March 25, 1994)

Abstract

A novel structure for a Si-based 2-terminal tandem solar cell was proposed. The structure was optimized to get high efficiency considering the realistic material parameters. Gallium arsenide phosphide ($GaAs_{1-x}P_x$) and indium gallium phosphide ($In_{1-x}Ga_xP$) were suggested as a top-cell material. A semi-empirical method was proposed to calculate the absorption coefficients of $GaAs_{1-x}P_x$ and $In_{1-x}Ga_xP$ at any value of the composition x. The conversion efficiency of the cell was calculated by simulating its voltage-current characteristics. It was shown that an efficiency of 33.1% can be obtained for a $GaAs_{.73}P_{.27}$/Si cell and 34.2% for an $In_{.57}Ga_{.43}P$/Si cell. $In_{1-x}Ga_xP$ was shown to be more promising because of its larger absorption coefficient than $GaAs_{1-x}P_x$'s.

1. Introduction

Single crystalline silicon (Si) is the most promising material for high-efficiency solar cells as a future energy source, because high-quality and large-area substrates can be easily obtained at a reasonable cost. Recently, there has been significant improvement in the conversion efficiency of Si solar cells, and the maximum of 23.1% (1 sun, A.M.1.5) has been attained experimentally.[1,2] To make sure that solar cells can be an energy source in the future, it is necessary to get an extremely high conversion efficiency of over 30%, which is higher than the limitation value of Si solar cells. In order to raise the efficiency of Si solar cells, a combination of a wide gap semiconductor with Si (a so-called "tandem" solar cell) is the most useful way, since it can utilize the solar spectrum in a wide range effectively.

There have been several reports on theoretical analyses of tandem solar cells.[3,4] In these analyses, the efficiency of tandem solar cells was examined[5] assuming that all photons with energies larger than the bandgap are absorbed and that there is no recombination loss. In experimental reports, AlGaAs/GaAs[6], InGaP/GaAs[7], and AlGaAs/Si[8,9] cells were fabricated and reported on. In these reports, conversion efficiencies over 27% were obtained for GaAs-based tandem

Department of Electrical Engineering II, Faculty of Technology, Kyoto University, Kyoto, 606-01, Japan

solar cells[6,7], but efficiencies of only about 18% were obtained for AlGaAs/Si cells[8,9], which is less than that of a Si single cell.

We suggested gallium arsenide phosphide ($GaAs_{1-x}P_x$) and indium gallium phosphide ($In_{1-x}Ga_xP$) as wide gap semiconductors, because their bandgaps can be easily adjusted to the range of 1.7～1.8eV, which is the most appropriate value for the top cell to combine with a Si cell[5], and because they can be grown continuously on a GaP buffer layer grown heteroepitaxially on Si, whose lattice-mismatch is very small (0.4%). We proposed a novel structure of a 2-terminal tandem solar cell, and examined its theoretical performance.[10] We precisely discussed the efficiency of the proposed cell considering the realistic material parameters such as absorption coefficient and diffusion length, and showed that a high efficiency of more than 30% can be obtained in the 2-terminal tandem structure.[10] In this paper, we discuss the simulation process in detail and show the device characteristics.

2. Novel structure

Figure 1 shows a schematic configuration of the proposed tandem solar cell. This structure consists of three parts, a top cell made of $GaAs_{1-x}P_x$ or $In_{1-x}Ga_xP$, a bottom cell made of a Si substrate, and a buffer layer between the top and the bottom cells which functions as a tunnel junction connecting the top and the bottom.

The top cell layer and the buffer layer are heteroepitaxially grown on the

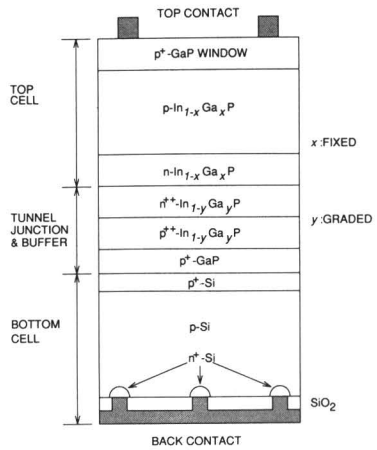

Fig. 1. Schematic configuration of proposed novel structure for 2-terminal Si tandem solar cell with $In_{1-x}Ga_xP$.

bottom Si cell. Such 2-terminal, or "monolithic", tandem solar cells can be connected with external circuits more easily than 4-terminal, or "mechanically stacked", tandem solar cells.

The bandgap of the semiconductor for the top cell can be easily controlled by changing the composition x. The proper bandgap can be optimized to get the highest efficiency under the condition of current continuity between the top and the bottom cells.

The buffer layer is made of $GaAs_{1-x}P_x$ or $In_{1-x}Ga_xP$ in accordance with the top-cell material. The composition x is the same as the top cell's just beneath it, and gradually increases from the top to the bottom. The layer just above the bottom Si cell is made of gallium phosphide (GaP) which is almost lattice-matched to Si. The layer is transparent to the light which passes through the top cell, because its bandgap is wider than that of the top cell. Therefore, the buffer layer can be made thicker, which suppresses crystalline defects due to the heteroepitaxial growth of the top cell layer, without significant loss in the light incident to the bottom cell.

A high-efficiency Si solar cell with very thin thickness (110μm) is used as the bottom cell. Bulk recombination loss is substantially decreased by the use of this cell. A deeply diffused and point-contacted pn^+ junction for carrier collection is formed at the rear surface. The area of junction can be reduced to about 1 percent of the whole cell area. It causes a reduction of the dark saturation current, and gives extremely high open circuit voltage. The front p^+-region is used as a potential barrier for the reduction of surface recombination velocity of minority carriers (electron) in the p-region.[11] A high conversion efficiency of 22% can be expected in the case of independent use. The performance of Si cells has been described elsewhere.[12]

In the next section, we establish the process to optimize the structure of tandem cells to get the highest efficiency. We design the optimum structure and estimate the highest efficiency which can be realized based on realistic material parameters such as absorption coefficient and minority carrier diffusion length.

3. Optimization of structure and examination of efficiency

3.1 Absorption coefficient of top-cell material

3.1.1 *Calculation model for absorption coefficients*

In a 2-terminal tandem solar cell, photo-generated currents in the top and the bottom cells must be equal. These currents are determined by photo-absorption and transmission of the top-cell material, which are derived from its

thickness and absorption coefficient $\alpha(\lambda)$.

To use an alloy semiconductor such as $GaAs_{1-x}P_x$ or $In_{1-x}Ga_xP$ for the top layer, the absorption coefficient $\alpha(\lambda)$ of a semiconductor with the composition x is required. The values of $\alpha(\lambda)$ of GaP[13], GaAs[14], and InP[15] were reported experimentally in a wide range of wavelengths, but those of $GaAs_{1-x}P_x$ and $In_{1-x}Ga_xP$ for a continuously-changed composition x have been rarely reported. We propose a new semi-empirical method to estimate the values of $\alpha(\lambda)$ for $GaAs_{1-x}P_x$ and $In_{1-x}Ga_xP$ in a wide range of x.

Figures 2 and 3 show the change of bandgaps for $GaAs_{1-x}P_x$[16] and $In_{1-x}Ga_xP$.[17] Two curves in each figure show Γ-point and X-point bandgaps which show direct and indirect transitions, respectively. These curves are derived as follows:

$$\left.\begin{aligned} E_{g1}^{\Gamma} &= 1.424 + 1.150x + 0.176x^2 \\ E_{g1}^{X} &= 1.810 + 0.306x + 0.145x^2 \end{aligned}\right\} : GaAs_{1-x}P_x{}^{16)}, \tag{1}$$

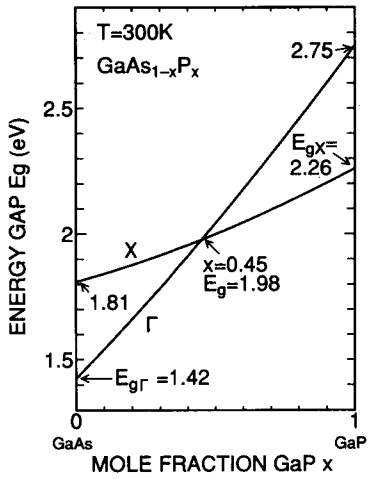

Fig. 2. Change of bandgaps of $GaAs_{1-x}P_x$ upon composition x.[16] The two curves show Γ-valley and X-valley bandgaps which show direct and indirect transitions, respectively.

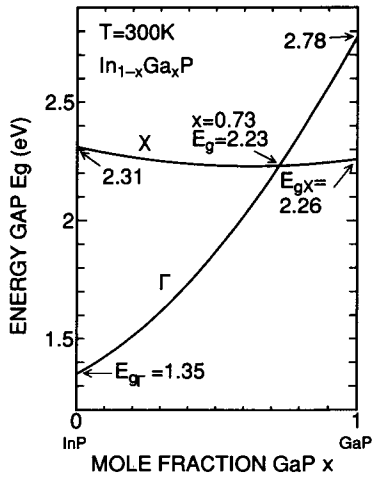

Fig. 3. Change of bandgaps of $In_{1-x}Ga_xP$ upon composition x.[17]

$$\left.\begin{aligned} E_{g2}^{\Gamma} &= 1.351 + 0.643x + 0.786x^2 \\ E_{g2}^{X} &= 2.311 - 0.2596x + 0.207x^2 \end{aligned}\right\} : \mathrm{In}_{1-x}\mathrm{Ga}_x\mathrm{P}^{17)}, \tag{2}$$

where E_g^{Γ} and E_g^{X} (eV) are Γ-point and X-point bandgaps, respectively, and subscripts 1 and 2 are for $GaAs_{1-x}P_x$ and $In_{1-x}Ga_xP$, respectively.

As seen in Figs. 2 and 3, the transition types of $GaAs_{1-x}P_x$ and $In_{1-x}Ga_xP$ vary with x, direct with smaller x and indirect with larger x. When the absorption coefficient $\alpha(\lambda)$ is considered, it is the sum of contributions from the direct and indirect transitions.

In general, absorption coefficient $\alpha(\lambda)$ has a relation with extinction coefficient $k(\lambda)$ as in the following:

$$\alpha(\lambda) = 4\pi k(\lambda)/\lambda. \tag{3}$$

From now on, the extinction coefficient $k(\lambda)$ will be mainly used for discussion about the absorption coefficient $\alpha(\lambda)$. Figure 4 shows the extinction coefficients of GaAs and GaP. The two solid lines in Fig. 4(a) show the reported extinction coefficients $k(\lambda)$ measured for GaAs[14] and GaP.[13] The points B_Γ and A_X show the wavelengths corresponding to the bandgaps of GaAs and GaP, respectively. The wavelength of the point $B_\Gamma(A_X)$ is 873(549)nm, derived from the following equation:

$$\lambda[\mathrm{nm}] = 1240/E[\mathrm{eV}]. \tag{4}$$

The extinction coefficient $k(\lambda)$ is considered to consist of $k_\Gamma(\lambda)$, which is contributed from the direct transition, and $k_X(\lambda)$, from the indirect transition. Thus, we assumed the relationship of $k(\lambda)$, $k_\Gamma(\lambda)$ and $k_X(\lambda)$ as follows:

$$k(\lambda) = k_\Gamma(\lambda) + k_X(\lambda). \tag{5}$$

The $k_\Gamma(\lambda)$ curve of GaAs can be expressed as follows by fitting the curve around the point B_Γ:

$$k_\Gamma(\lambda)_{\mathrm{GaAs}} = \begin{cases} 10^{-1.3-0.0022(\lambda-873)}, & (\lambda < 873), \\ 10^{-1.3-0.084(\lambda-873)}, & (\lambda > 873). \end{cases} \tag{6}$$

These two equations express the curve bending sharply at the point B_Γ.

In the same way, the $k_X(\lambda)$ curve of GaP can be expressed as follows by fitting the curve around the point A_X:

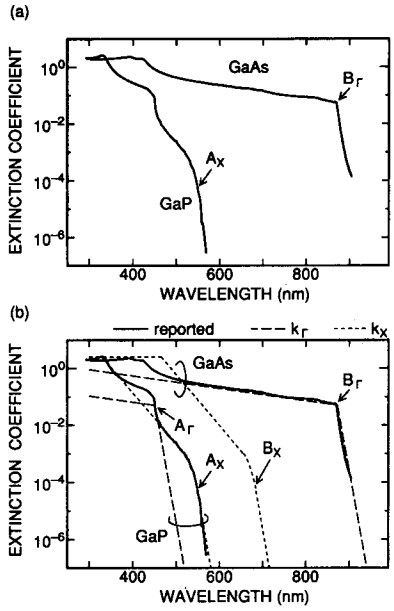

Fig. 4. Wavelength-dependence of extinction coefficients $k(\lambda)$ of GaAs and GaP. (a) Reported values of GaAs and GaP. (b) Calculated values of $k_\Gamma(\lambda)$ and $k_X(\lambda)$ together with reported values, based on our assumption. Two solid lines represent reported values. Dashed and dotted lines represent $k_\Gamma(\lambda)$ and $k_X(\lambda)$, respectively. The point A_Γ shows the Γ-valley bandgap of GaP, and the point A_X the X-valley one. The point B_Γ and B_X are for GaAs. The wavelengths of the points A_Γ, A_X, B_X, and B_Γ are 451, 549, 685, and 873 nm, respectively.

$$k_X(\lambda)_{GaP}=\begin{cases}10^{-3.0-0.018(\lambda-549+30)}, & (\lambda<549-30),\\ 10^{-3.0-0.0053(\lambda-549+30)^{1.6}}, & (549-30<\lambda<549),\\ 10^{-4.3-0.087(\lambda-549)}, & (\lambda>549).\end{cases} \tag{7}$$

These three equations express the curve bending gently at the point A_X. The second equation in eq. (7) expresses the region bending gently, assuming that the range of the region is 30nm.

If the $k_\Gamma(\lambda)$ curve of GaP can be assumed to be given by a parallel-shifted curve of eq. (6) from $\lambda=873$nm to 451nm without changing the values of the vertical axis, it is expressed as follows:

$$k_\Gamma(\lambda)_{GaP}=\begin{cases}10^{-1.3-0.0022(\lambda-451)}, & (\lambda<451),\\ 10^{-1.3-0.084(\lambda-451)}, & (\lambda>451).\end{cases} \tag{8}$$

Here, the wavelength 451nm corresponds to the Γ-valley bandgap of GaP (2.75eV).

If the same assumption holds for the $k_X(\lambda)$ curve of GaAs, it is expressed as follows by parallel-shifting the curve of eq. (7) from $\lambda=549$nm to 685nm:

$$k_X(\lambda)_{GaAs}=\begin{cases}10^{-3.0-0.018(\lambda-685+30)}, & (\lambda<685-30),\\ 10^{-3.0-0.0053(\lambda-685+30)^{1.6}}, & (685-30<\lambda<685),\\ 10^{-4.3-0.087(\lambda-685)}, & (\lambda>685).\end{cases} \tag{9}$$

Here, the wavelength 685nm corresponds to the X-valley bandgap of GaAs (1.81eV).

Figure 4(b) shows the calculated extinction coefficients of eqs. (6)~(9) with the reported values of GaAs and GaP in Fig. 4(a). The solid lines represent reported values, and dashed and dotted lines represent calculated $k_\Gamma(\lambda)$ and $k_X(\lambda)$, respectively. The wavelengths of point A_Γ and B_X are 451 and 685nm, respectively. Figure 4(b) shows that $k_\Gamma(\lambda)+k_X(\lambda)$, eqs. (6)+(9) or eqs. (7)+(8), are roughly equal to the reported values for both GaAs and GaP, so the assumption of eq. (5) mostly holds. Therefore, these assumptions are considered to be appropriate for GaAs and GaP.

If these assumptions hold for $GaAs_{1-x}P_x$ with any value of composition x, $k_\Gamma(\lambda)$ and $k_X(\lambda)$ of $GaAs_{1-x}P_x$ are expressed as follows:

$$k_\Gamma(\lambda)_{GaAs_{1-x}P_x}=\begin{cases}10^{-1.3-0.0022(\lambda-\lambda_{g1}^{\Gamma})}, & (\lambda<\lambda_{g1}^{\Gamma}),\\ 10^{-1.3-0.084(\lambda-\lambda_{g1}^{\Gamma})}, & (\lambda>\lambda_{g1}^{\Gamma}).\end{cases} \tag{10}$$

$$k_X(\lambda)_{GaAs_{1-x}}=\begin{cases}10^{-3.0-0.018(\lambda-\lambda_{g1}^{X}+30)}, & (\lambda<\lambda_{g1}^{X}-30),\\ 10^{-3.0-0.0053(\lambda-\lambda_{g1}^{X}+30)^{1.6}}, & (\lambda_{g1}^{X}-30<\lambda<\lambda_{g1}^{X}),\\ 10^{-4.3-0.087(\lambda-\lambda_{g1}^{X})}, & (\lambda>\lambda_{g1}^{X}).\end{cases} \tag{11}$$

where λ_{g1}^{Γ} and λ_{g1}^{X} are the wavelengths corresponding to E_{g1}^{Γ} and E_{g1}^{X} in eq. (1).

Figure 5 shows a comparison between the curves of extinction coefficient $k(\lambda)$ calculated by this procedure and the measured values.[18] The measured absorption coefficients were converted to extinction coefficients using eq. (3) The calculated curves fit well with experimentally obtained values, which shows that the procedure is appropriate. Using eqs. (3), (5), (10), and (11), the absorption coefficients $\alpha(\lambda)$ of $GaAs_{1-x}P_x$ with any values of x can be calculated for a wide range of λ.

Similarly, $In_{1-x}Ga_xP$, $k_\Gamma(\lambda)$ and $k_X(\lambda)$ for any values of composition x are obtained. Figure 6(a) shows the extinction coefficients $k(\lambda)$ of InP[15] and

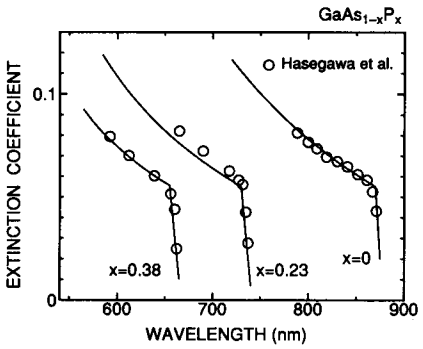

Fig. 5. Comparison between calculated curves based on our assumption and measured values by Hasegawa *et al.*[18]

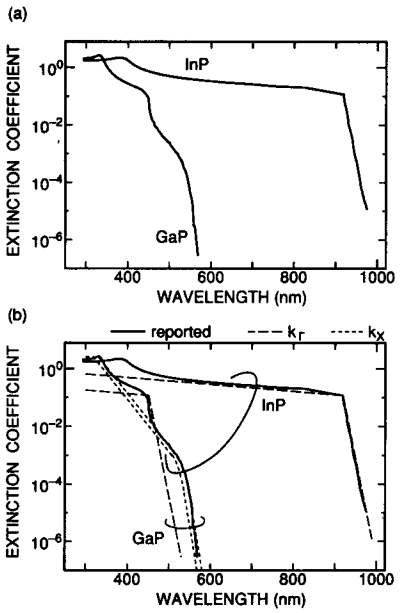

Fig. 6. Wavelenth-dependence of extinction coefficients $k(\lambda)$ of InP and GaP. (a) Reported values of InP and GaP. (b) Calculated values of $k_\Gamma(\lambda)$ and $k_X(\lambda)$ with measured values, based on our assumption.

GaP.[13] The $k_\Gamma(\lambda)$ curve of InP can be expressed as follows by fitting:

$$k_\Gamma(\lambda)_{InP}=\begin{cases}10^{-0.93-0.0012(\lambda-919)}, & (\lambda<919),\\ 10^{-0.93-0.071(\lambda-919)}, & (\lambda>919).\end{cases} \tag{12}$$

And the $k_X(\lambda)$ curve of InP can be expressed as follows by parallel-shifting the curve of eq. (7) from $\lambda=549$nm to 537nm:

$$k_X(\lambda)_{InP}=\begin{cases}10^{-3.0-0.018(\lambda-537+30)}, & (\lambda<537-30),\\ 10^{-3.0-0.0053(\lambda-537+30)^{1.6}}, & (537-30<\lambda<537),\\ 10^{-4.3-0.087(\lambda-537)}, & (\lambda>537).\end{cases} \tag{13}$$

Here, the wavelength 537nm corresponds to the X-valley bandgap of InP (2.31eV). Therefore, $k_\Gamma(\lambda)$ and $k_X(\lambda)$ for $In_{1-x}Ga_xP$ are expressed as follows:

$$k_\Gamma(\lambda)_{In_{1-x}Ga_xP}=\begin{cases}10^{-0.93-0.0012(\lambda-\lambda_{g2}^\Gamma)}, & (\lambda<\lambda_{g2}^\Gamma),\\ 10^{-0.93-0.071(\lambda-\lambda_{g2}^\Gamma)}, & (\lambda>\lambda_{g2}^\Gamma).\end{cases} \tag{14}$$

$$k_X(\lambda)_{In_{1-x}Ga_xP}=\begin{cases}10^{-3.0-0.018(\lambda-\lambda_{g2}^X+30)}, & (\lambda<\lambda_{g2}^X-30),\\ 10^{-3.0-0.0053(\lambda-\lambda_{g2}^X+30)^{1.6}}, & (\lambda_{g2}^X-30<\lambda<\lambda_{g2}^X),\\ 10^{-4.3-0.087(\lambda-\lambda_{g2}^X)}, & (\lambda>\lambda_{g2}^X).\end{cases} \tag{15}$$

Figure 6(b) shows the $k_\Gamma(\lambda)$ and $k_X(\lambda)$ curves of InP and GaP with the reported values. Therefore, for $In_{1-x}Ga_xP$, the absorption coefficients $\alpha(\lambda)$ can be calculated, but there has been no report on measurements.

3.1.2 Photo-generated current

Using these calculated values of absorption coefficients, photo-generated current densities in the top and the bottom cells were roughly estimated. Two simple assumptions were used: carriers are generated only in the *p*-active layers of both the top and the bottom cells, and there is no recombination loss. The solar spectrum used in this calculation for the top cell is A.M. 1.5, $100mW\cdot cm^{-2}$.[19] For the bottom Si cell, the spectrum was modified as follows assuming no reflection loss at the interface:

$$F^\phi(\lambda)=F^t(\lambda)e^{-\alpha^t(\lambda)(w_p{}^t+w_n{}^t)}, \tag{16}$$

where $F^\phi(\lambda)(nm^{-1})$ is the number of photons incident to the bottom cell per unit

wavelength, $F^t(\lambda)$ is that of A.M. 1.5 (incident to the top cell), and w_p^t and w_n^t are the thicknesses of p- and n-layers of the top-cell, respectively.

Figure 7 shows the w_p^t (top-cell active layer thickness) dependence of photo-generated current densities in both the top and the bottom cells when the top cell material is $GaAs_{1-x}P_x$. The phosphorus composition x of each figure is (a)$x=1$ (GaP), (b)$x=0.33$ ($GaAs_{.67}P_{.33}$), and (c)$x=0$ (GaAs). With decreasing phosphorus composition, the bandgap becomes narrow. As seen in Fig. 7(a), the generated current in the top cell is much less than that in the bottom cell even for a large w_p^t, because the bandgap of the top cell is too wide to absorb enough photons. In Fig. 7(b), the currents in the top and the bottom cells are almost equal for $w_p^t \approx 10\mu$m. It is shown, by comparing Figs. 7(a) and (b), that there is no w_p^t where both currents become equal when the phosphorus composition x is in the range of $0.33<x<1$. On the contrary, in Fig. 7(c) both currents are equal when $w_p^t \approx 0.3\mu$m, and they will become equal in a certain value ($0.3 \sim 10\mu$m)of w_p^t when the phosphorus composition x is in the range of $0<x<0.33$. As described in the beginning of this section, photo-generated currents in the top and the bottom cells must be equal in a 2-terminal tandem solar cell. Figure 7 shows that this condition is satisfied in the case of $x<0.33$. Then, the transition type of $GaAs_{1-x}P_x$ is direct, and the bandgap E_g is less than 1.82eV.

Similarly, Fig. 8 shows the case in which the top cell material is

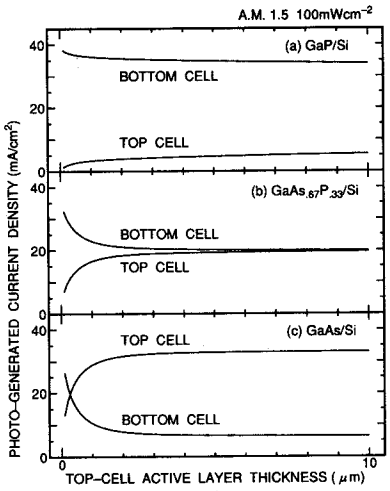

Fig. 7. Photo-generated current densities vs. top-cell active layer thickness (w_p^t) of $GaAs_{1-x}P_x$/Si cell assuming no recombination loss, (a) $x=1$ (GaP), (b) $x=0.33$ ($GaAs_{.67}P_{.33}$), and (c) $x=0$ (GaAs).

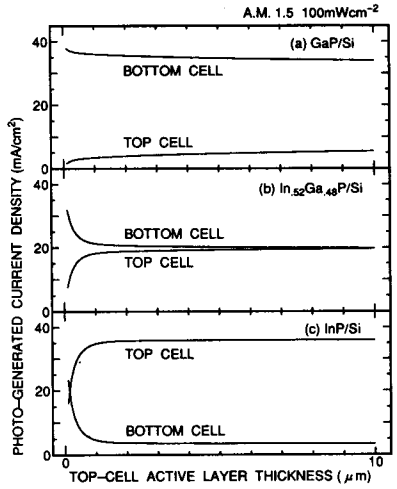

Fig. 8. Photo-generated current densities vs. top-cell active layer thickness of $In_{1-x}Ga_xP$/Si cell. (a) $x=1$ (GaP), (b) $x=0.48$ ($In_{.52}Ga_{.48}P$), and (c) $x=0$ (InP).

$In_{1-x}Ga_xP$. The gallium composition x of each figure is (a)$x=1$ (GaP), (b)$x=0.48$ ($In_{.52}Ga_{.48}P$), and (c)$x=0$ (GaAs). The same as in the case of $GaAs_{1-x}P_x$, with decreasing gallium composition x, the bandgap becomes narrower. The generated currents in the top and the bottom cells become equal at a certain value of thickness for $0<x<0.48$. In this case, the transition type of $In_{1-x}Ga_xP$ is direct, and the E_g is less than 1.84eV.

3.2 Optimization of structure

Using the calculated values of $\alpha(\lambda)$ and the thickness w_p^t of the top-cell active layer which absorbs the solar light, the spectra passed through and absorbed in the active layer were calculated. The generated current density $J_e(\lambda)$ per unit wavelength in the p-active layer can be calculated in the following equation[a] similarly for both the top and the bottom cells,

$$J_e(\lambda)=\frac{\alpha(\lambda)qF(\lambda)L_e}{\alpha(\lambda)^2L_e^2-1}\left[\alpha(\lambda)L_e\{e^{-\alpha(\lambda)w_p}-R_be^{-\alpha(\lambda)(2w^b-w_p)}\}-\frac{\alpha(\lambda)L_e(1-R_be^{-2\alpha(\lambda)w^b})}{\frac{S_eL_e}{D_e}\sinh\frac{w_p}{L_e}+\cosh\frac{w_p}{L_e}}\right.$$

$$\left.-\left\{\frac{S_eL_e}{D_e}(1+R_be^{-2\alpha(\lambda)w^b})-\left(e^{-\alpha(\lambda)w_p}+R_be^{-\alpha(\lambda)(2w^b-w_p)}\right)\left(\frac{S_eL_e}{D_e}\cosh\frac{w_p}{L_e}+\sinh\frac{w_p}{L_e}\right)\right\}\right]$$

[a]See Appendix

$$\times\left(\frac{S_eL_e}{D_e}\sinh\frac{w_p}{L_e}+\cosh\frac{w_p}{L_e}\right)\Bigg], \tag{17}$$

where, q is the electronic charge, L_e, D_e, and S_e are the diffusion length, the diffusion constant, and the surface recombination velocity (SRV) of electrons in the p-active layer, respectively, and w^b is the bottom cell thickness. R_b is the reflectivity of the rear surface and the value is assumed to be 0.97 for the bottom cell and 0 for the top. $F(\lambda)$ for the top cell is that of A.M.1.5, 100mW·cm^{-2}, and that for the bottom cell is the modified one given by eq. (16). The generated current in the n^+-layer is much smaller than $J_e(\lambda)$, so it can be ignored. The short circuit current I_{sc} can be calculated by integrating $J_e(\lambda)$ for the spectrum and multiplying the cell area.

Assuming no series resistance loss, the open circuit voltage V_{oc} is derived as follows:

$$V_{oc}=\frac{nkT}{q}\ln\left(\frac{I_{sc}+I_0}{I_0}\right), \tag{18}$$

where n is the ideality factor of pn junction, and I_0 is the dark saturation current, respectively. The value of I_0 is proportional to the area of pn junction, so I_0 of the bottom cell becomes very small.

Table 1 Some important parameters used in this calculation.

	Top cell		Bottom Si cell	
	p	n	p	n
Thick.	0.5~2.0	0.1	110	1.5
Dop.	1×10^{16}	3×10^{19}	1×10^{16}	3×10^{19}
S.R.V.	10	1×10^{6}	10	1×10^{6}
D.L.	4.2	0.089	590	0.78

Thick.: Thickness (μm)
Dop.: Dopant concentration (cm^{-3})
S.R.V. Surface recombination velocity (cm/s)
D.L.: Diffusion length (μm)

The product of short circuit current I_{sc} and open circuit voltage V_{oc} was calculated. Table 1 shows some important parameters used in this calculation. The diffusion length L_e of minority carriers (electron) for the top cell is assumed to be a realistic one: it followed consideration in the case of GaAs with various impurity concentrations. The surface recombination velocity of 10cm/s is supposed considering the effect of potential barrier at the front side.[11]

The composition x and the thickness $w_p{}^t$ were optimized by considering the current continuity condition between the top and the bottom cells.

Figure 9 shows the product $I_{sc}V_{oc}$ of a $1cm^2$ cell as a function of $w_p{}^t$ with changing x in the case of $GaAs_{1-x}P_x$. On some curves in the figure, there are "kink" points. These points show that I_{sc} of the top and the bottom cells become equal there. On the left side of the "kink" points, $w_p{}^t$ is thin, and I_{sc} of the top cell is less than that of the bottom cell. So I_{sc} of the whole cell is limited by that of the top cell. On the right side, $w_p{}^t$ is too thick and I_{sc} of the top cell becomes larger than that of the bottom cell, and I_{sc} of the whole cell is limited by that of the bottom cell. On the curves for $x>0.27$, I_{sc} of the top cell does not exceed that of the bottom cell and there appears no "kink" point. The optimum condition to get the highest efficiency is where $I_{sc}V_{oc}$ becomes maximal, and it must be one of the "kink" points. The conditions for $GaAs_{1-x}P_x$ are $x=0.27$, $w_p{}^t=1.73\mu m$ as shown in Fig. 9.

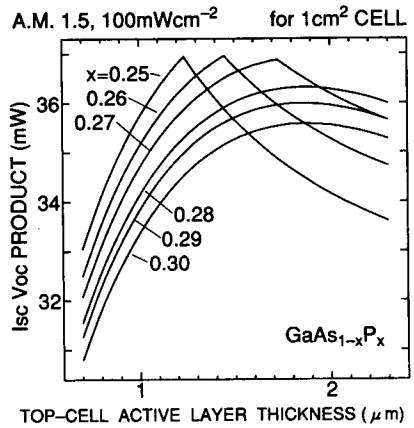

Fig. 9. Product $I_{sc}V_{oc}$ vs. top-cell active layer thickness $w_p{}^t$ of $GaAs_{1-x}$-P_x/Si cell. "Kink" points show that I_{sc} of top and bottom cells become equal there. The point where the product is maximal shows the optimum values of x and $w_p{}^t$, which are $x=0.27$, $w_p{}^t=1.73$ μm in this figure.

Figure 10 shows the product $I_{sc}V_{oc}$ as a function of $w_p{}^t$ in the case of $In_{1-x}Ga_xP$. This figure shows the same tendency as Fig. 9, and it shows the optimum condition for $In_{1-x}Ga_xP$: $x=0.43$ and $w_p{}^t=0.92\mu m$.

The voltage-current characteristics of the cell were simulated using the optimum structure designed above, and the energy conversion efficiency was figured out. In this structure, it is considered that the two *pn* junctions of the top and the bottom cells are connected in series and that the tunnel junction is assumed to be a simple resistance whose value is about 0.5Ω. The voltage V^a of the whole cell at current I was calculated as follows:

$$V^a(I)=V^t(I)+V^b(I)-R_{tun}I, \tag{19}$$

where V^t and V^b are the voltages of the top and the bottom cells, respectively, and R_{tun} is the resistance of the tunnel junction. The conversion efficiency η and fill factor FF were calculated from the maximum of product V^aI following eq. (19). The relation of V to I for each cell was calculated from the following equation of voltage-current relationship:

$$V(I)=\frac{nkT}{q}\ln\left(\frac{I_{sc}+I_0-I}{I_0}\right)-R_sI, \tag{20}$$

where R_s is the series resistance including the tunnel resistance.

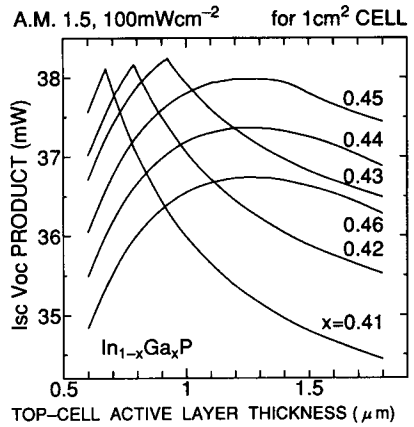

Fig. 10. Product $I_{sc}V_{oc}$ vs. top-cell active layer thickness $w_p{}^t$ of $In_{1-x}Ga_x$-P/Si cell. The optimum values of x and $w_p{}^t$ are $x=0.43$, $w_p{}^t=0.92\mu m$.

Figure 11 shows the result of simulation of the voltage-current characteristics in the $In_{.57}Ga_{.43}P$/Si 2-terminal tandem solar cell using eq. (19). In this figure, the dashed, dotted, and solid lines show the characteristics of top cell, bottom cell, and whole cell, respectively. Efficiency η and fill factor FF can be calculated from the product V^aI on this solid line. The results of this simulation shown in Table 2 were obtained in the case of the optimum conditions derived from Figs. 9 and 10. The conversion efficiency is 33.1% and 34.3% when $GaAs_{.73}P_{.27}$ and $In_{.57}Ga_{.43}P$ are used, respectively.

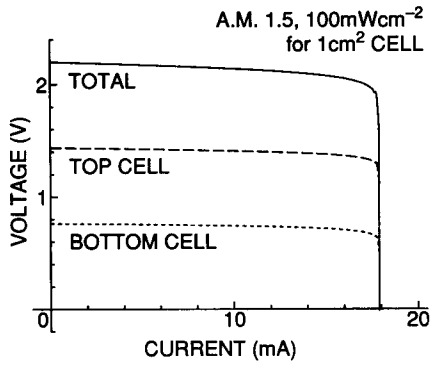

Fig. 11. Simulation result of voltage-current characteristics in $In_{.57}Ga_{.43}P$/Si 2-terminal tandem solar cell. Dashed, dotted, and solid lines show characteristics of top cell, bottom cell, and whole cell.

Table 2. Results of simulation (1 cm^2 cell).

Top cell	$GaAs_{.73}P_{.27}$	$In_{.57}Ga_{.43}P$
$w_p{}^t$ (μm)	1.73	0.92
E_g (eV)	1.75	1.77
I_{sc} (mA)	17.8	17.9
V_{oc} (mV)	2140	2200
(top)	(1380)	(1440)
(bot.)	(760)	(760)
FF	0.87	0.87
η (%)	33.1	34.3

4. Discussion

The reason why $In_{.57}Ga_{.43}P$ shows higher efficiency than $GaAs_{.73}P_{.27}$ is explained as follows: Figure 12 shows the calculated $\alpha(\lambda)$ near the absorption edge of $GaAs_{.73}P_{.27}$ and $In_{.57}Ga_{.43}P$. The value of α for $In_{.57}Ga_{.43}P$ is about two times larger than that for $GaAs_{.73}P_{.27}$, and so w_p^t for $In_{.57}Ga_{.43}P$ is required to be only a half of that for $GaAs_{.73}P_{.27}$ to get enough I_{sc}. The reduction of w_p^t leads to a decrease in I_0, and it contributes to the increase in V_{oc}. Therefore, higher efficiency can be obtained when $In_{.57}Ga_{.43}P$ is used as the top-cell material.

The influence of electron diffusion length L_e in the p-layer of the top cell upon η was considered. Figure 13 shows the relationship of η to L_e when $GaAs_{1-x}P_x$ and $In_{1-x}Ga_xP$ are used as the top-cell material. It is shown that the reduction in L_e leads to a decrease in η for both materials. When L_e changes from 5μm to 1μm, η goes down from 33.4% to 30.9% (2.5points) for $GaAs_{1-x}P_x$, but for $In_{1-x}Ga_xP$, η goes down by only 1.5point, from 34.4% to 32.9%. The influence of a reduction in L_e upon η is smaller for $In_{1-x}Ga_xP$ than for $GaAs_{1-x}P_x$, because the p-layer can be thinner owing to a larger α, and I_{sc} decreases slightly even if L_e becomes short.

From the above discussion, high efficiency of more than 34% can be expected for a Si-based 2-terminal tandem solar cell. It is shown that $In_{1-x}Ga_xP$ is more promising as the top-cell material than $GaAs_{1-x}P_x$.

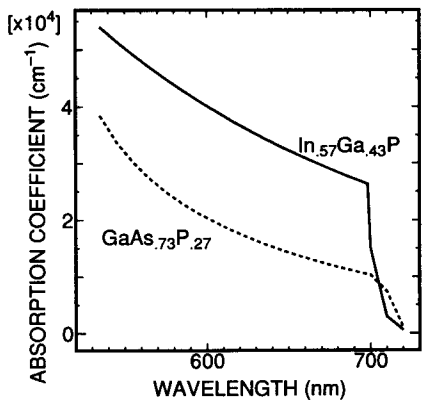

Fig. 12. Calculated absorption coefficient $\alpha(\lambda)$ of $GaAs_{.73}P_{.27}$ and $In_{.57}Ga_{.43}P$ around absorption edge. Values of $In_{.57}Ga_{.43}P$ are about two times larger than that of $GaAs_{.73}P_{.27}$.

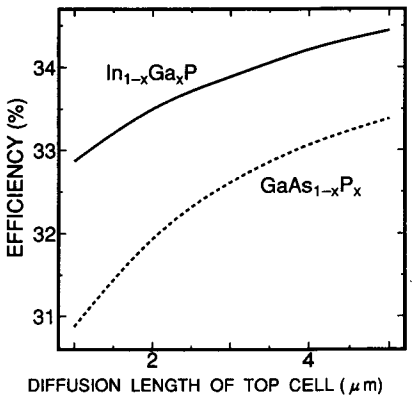

Fig. 13. Efficiency vs. electron diffusion length L_e of top-cell p-layer for $GaAs_{1-x}P_x$/Si and $In_{1-x}Ga_xP$ cell. L_e influence for $In_{1-x}Ga_xP$/Si cell is smaller than that for $GaAs_{1-x}P_x$/Si cell.

5. Conclusion

We proposed a novel structure of a Si-based 2-terminal tandem solar cell, and optimized the structure of the top cell to get the highest efficiency. We also estimated realizable energy conversion efficiency by device simulation. These calculations made the followings clear:

(1) The optimum structure of a 2-terminal tandem solar cell was designed to get the highest efficiency using realistic material parameters such as absorption coefficient, diffusion length, and so on.

(2) A semi-empirical method was proposed to calculate the absorption coefficient $\alpha(\lambda)$ of $GaAs_{1-x}P_x$ and $In_{1-x}Ga_xP$ at any value of the composition x. The method was shown to be closely appropriate by comparison with experimental data for $GaAs_{1-x}P_x$.

(3) The conversion efficiency of the 2-terminal tandem solar cell was calculated by the simulation of the voltage-current characteristics, and it is shown that the efficiency is 33.1% and 34.2% when $GaAs_{.73}P_{.27}$ and $In_{.57}Ga_{.43}P$ are used, respectively.

(4) The absorption coefficients of $In_{.57}Ga_{.43}P$ near the absorption edge are larger than those of $GaAs_{.73}P_{.27}$, and the top-cell active layer can be thinner for $In_{.54}Ga_{.43}P$, which leads to higher open circuit voltage. Besides, the $In_{.54}Ga_{.43}P$ cell is less affected by the reduction of diffusion length. $In_{1-x}Ga_xP$ is considered more promising for high efficiency.

Acknowledgments

This work was partially supported by a Grant-in-Aid on Priority-Area Research, "Energy Conversion and Utilization with High Efficiency," from the Ministry of Education, Science and Culture.

References

[1] A. Wang, J. Zhao and M. A. Green; Appl. Phys. Lett., **57**, pp. 602–4 (1990).
[2] M. A. Green and K. Emery; Prog. in Photovolt., Res. Appl., **1**, pp. 25–9 (1993).
[3] J. C. C. Fan, B. Y. Tsaur and B. J. Palm; Conf. Rec. of 16th IEEE Photovoltaic Specialists Conf., pp. 692–701 (1982).
[4] M. E. Nell and A. M. Barnett; Conf. Rec. of 18th IEEE Photovoltaic Specialists Conf., pp. 116–21 (1985).
[5] M. E. Nell and A. M. Barnett; IEEE Electron. Devices, **ED-34**, pp. 257–66 (1987).
[6] B. C. Chung, G. F. Virshup, S. Hikido and N. R. Kaminar; Appl. Phys. Lett., **55**, pp. 1741–3 (1989).
[7] J. M. Olson, S. R. Kurtz, A. E. Kibbler and P. Faine; Appl. Phys. Lett., **56**, pp. 623–5 (1990).
[8] H. Shimizu, T. Egawa, T. Soga, T. Jimbo and M. Umeno; Jpn. J. Appl. Phys., **31**, pp.

L1150—2 (1992).
[9] Y. Ohmachi, T. Ohara and Y. Kadota; Conf. Rec. of 21st IEEE Photovoltaic Specialists Conf., pp. 89–94 (1990).
[10] Y. Komatsu, T. Fuyuki and H. Matsunami; Technical Digest of the Int'l. PVSEC–5, pp. 443–6 (1990).
[11] T. Saitoh and H. Hasegawa; Jpn. J. Appl. Phys., **29**, pp. L2296–9 (1990).
[12] T. Fuyuki, Y. Komatsu and H. Matsunami; Technical Digest of the Int'l. PVSEC–5, pp. 591–4 (1990).
[13] A. Borghesi and G. Guizzetti; "Handbook of Optical Constants of Solids", pp. 445–64, Academic Press (1985).
[14] E. D. Palik; "Handbook of Optical Constants of Solids", pp. 429–43, Academic Press (1985).
[15] O. J. Glembocki and H. Peller; "Handbook of Optical Constants of Solids", pp. 503–16, Academic Press (1985).
[16] A. G. Thompson, M. Cardona, K. L. Shaklee and J. C. Woolley; Phys. Rev., **146**, pp. 601–10 (1966).
[17] R. J. Nelson and N. Holonyak, Jr.; J. Phys. Chem. Solids, **37**, pp. 629–37 (1976).
[18] S. Hasegawa, A. Tanaka and T. Sukegawa; J. Appl. Phys., **55**, pp. 3188–9 (1984).
[19] Special Committee for Solar Cell Investigation, Denki-Gakkai Ed.; "Taiyo Denchi Hando-Bukku (Solar Cell Handbook)", p. 221, Denki-Gakkai, 12–1, Yuuraku-cho 1-chome, Chiyoda-ku, Tokyo (1985); [*in Japanese*].

Appendix

Here, we explain how to deduce eq. (17).

When monochromatic light with wavelength λ is incident to a cell with thickness w from a p-type layer, the generation rate $G(\lambda,z)$ of electron-hole pairs at length z from the surface can be expressed as follows assuming no reflection loss at the surface:

$$G(\lambda,z)=\alpha(\lambda)F(\lambda)(e^{-\alpha(\lambda)z}+R_b e^{-\alpha(\lambda)(2w-z)}), \tag{A.1}$$

where $F(\lambda)$ is the number of photons of monochromatic light, $\alpha(\lambda)$ is the absorption coefficient of the cell, and R_b is the back surface reflectance.

The 1-dimensional current continuity condition of electrons in the p-layer under the steady-state condition is expressed as follows:

$$G(\lambda,z)-\frac{n_p(\lambda,z)-n_{p0}}{\tau_e}+\frac{1}{q}\frac{d}{dz}J_e(\lambda,z)=0, \tag{A.2}$$

where $n_p(\lambda,z)$ is the electron concentration, n_{p0} that in an equilibrium condition, τ_e electron lifetime, and $J_e(\lambda,z)$ the electron current density.

$J_e(\lambda,z)$ is expressed as follows, exclusive of electric field:

$$J_e(\lambda,z)=qD_e\frac{d}{dz}n_p(\lambda,z), \tag{A.3}$$

where D_e is the diffusion constant of electron.

The boundary condition at the surface ($z=0$) for eqs. (A.2) and (A.3) can be expressed as follows:

$$D_e\frac{d}{dz}\{n_p(\lambda,0)-n_{p0}\}=S_e\{n_p(\lambda,0)-n_{p0}\}, \tag{A.4}$$

where S_e is the surface recombination velocity (SRV) of electron. Assuming that the depletion layer between p- and n-layers is thin enough to be ignored, the p-layer thickness without the depletion layer is almost equal to the original p-layer thickness w_p, so the boundary condition at the depletion layer edge ($z=w_p$) can be expressed as follows:

$$n_p(w_p)-n_{p0}=0. \tag{A.5}$$

By solving eqs. (A.1)–(A.5), electron current density $J_e(\lambda)$ at the depletion

layer edge ($z=w_p$)is found to be as follows:

$$J_e(\lambda)=\frac{\alpha(\lambda)qF(\lambda)L_e}{\alpha(\lambda)^2L_e^2-1}\left[\alpha(\lambda)L_e\{e^{-\alpha(\lambda)w_p}-R_be^{-\alpha(\lambda)(2w-w_p)}\}-\frac{\alpha(\lambda)L_e(1-R_be^{-2\alpha(\lambda)w})}{\frac{S_eL_e}{D_e}\sinh\frac{w_p}{L_e}+\cosh\frac{w_p}{L_e}}\right.$$
$$-\left\{\frac{S_eL_e}{D_e}(1+R_be^{-2\alpha(\lambda)w})-\left(e^{-\alpha(\lambda)w_p}+R_be^{-\alpha(\lambda)(2w-w_p)}\right)\left(\frac{S_eL_e}{D_e}\cosh\frac{w_p}{L_e}+\sinh\frac{w_p}{L_e}\right)\right\}$$
$$\left.\times\left(\frac{S_eL_e}{D_e}\sinh\frac{w_p}{L_e}+\cosh\frac{w_p}{L_e}\right)\right], \tag{A.6}$$

where L_e is the diffusion length of electron. This value represents the photo-generated current in the p-layer.